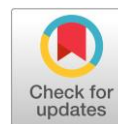


## Effect of Sn doping on sinterability and electrical conductivity of strontium hafnate

Adelya S. Khaliullina\* , Anastasia N. Meshcherskikh ,  
Liliya A. Dunyushkina 

Laboratory of Electrochemical Material Science, Institute of High Temperature Electrochemistry,  
Ekaterinburg 620066, Russia

\* Corresponding author: [Adeliao1@mail.ru](mailto:Adeliao1@mail.ru)



This paper belongs to a Regular Issue.

### Abstract

The effect of isovalent substitution of hafnium by tin in strontium hafnate on sinterability and electrical conductivity was studied for the first time. The ceramic samples  $\text{SrHf}_x\text{Sn}_{1-x}\text{O}_{3-\delta}$  ( $x = 0-0.16$ ) were synthesized by solid-state reaction and sintered at 1600 °C for 5 h. The samples were examined using the methods of X-ray diffraction, scanning electron microscopy, impedance spectroscopy, and four-probe direct current technique. It was shown that all samples were phase pure and had the orthorhombic structure of  $\text{SrHfO}_3$  with the *Pnma* space group. Sn doping resulted in an increase in grain size, relative density and conductivity; the sample with  $x = 0.08$  demonstrated the highest conductivity, which was ~830 times greater than that of undoped strontium hafnate at 600 °C. The conductivity of  $\text{SrHf}_{0.92}\text{Sn}_{0.08}\text{O}_{3-\delta}$  was  $4.1 \cdot 10^{-6} \text{ S cm}^{-1}$  at 800 °C in dry air. The possible reasons for the effect of Sn on the electrical properties of strontium hafnate were discussed.

### Keywords

strontium hafnate  
perovskite  
electrical conductivity  
electrolyte

Received: 16.02.23

Revised: 13.03.23

Accepted: 14.03.23

Available online: 17.03.23

### Key findings

- Ceramic samples  $\text{SrHf}_x\text{Sn}_{1-x}\text{O}_{3-\delta}$  ( $x = 0-0.16$ ) were obtained by the solid-phase method.
- Sn doping enhances the sintering ability of ceramics.
- Sn doping results in an increase in conductivity by more than 2 orders of magnitude.

© 2023, the Authors. This article is published in open access under the terms and conditions of the Creative Commons Attribution (CC BY) license (<http://creativecommons.org/licenses/by/4.0/>).

### 1. Introduction

Complex oxides with the  $\text{ABO}_3$  perovskite structure are of interest as functional elements of electronics, thermal barrier coatings, electrolytes and electrodes for high-temperature electrochemical applications [1-7]. In the 1980s, compounds capable of proton transfer were discovered among perovskites [8-11], and since then, active research has been carried out in the field of developing perovskites with high proton conductivity. Among perovskite-like oxides of the  $\text{A}^{2+}\text{B}^{4+}\text{O}_3$  type, the materials based on  $\text{BaCeO}_3$  and  $\text{SrCeO}_3$  exhibit the highest proton conductivity [12-16], but their use in electrochemical cells is hindered by their low chemical resistance to carbon dioxide. Zirconates and hafnates of alkaline earth metals are characterized by high chemical stability, which makes them promising for practical applications, and possess oxide-ion and proton conductivity; however, the ionic conductivity of these materials is low [17-21]. It is known that the substitutions in A and B

positions affect many characteristics of  $\text{ABO}_3$  perovskites; therefore, this approach is widely used to modify the ionic conductivity. As a rule, the method of acceptor doping is used, which makes it possible to increase the concentration of oxygen vacancies and, accordingly, the ionic conductivity [20-25]. In addition, doping is a common approach to improving the sinterability of solid oxides. Solid oxide electrolytes, including those with a perovskite structure, are refractory materials, which are sintered at very high temperatures [28-34].

Yamanaka et al. [26] reported on the fabrication of ceramic samples of  $\text{SrHfO}_3$  with the relative density of 94% by the solid state method, followed by the prolonged sintering at 1600 °C for 10 h. Qian et al. [29] used alumina as sintering aid to increase the density of Ce-doped  $\text{SrHfO}_3$  ceramics. The powders of  $\text{Sr}_{0.995}\text{Ce}_{0.005}\text{HfO}_3$  and  $\text{Sr}_{0.995}\text{Ce}_{0.005}\text{Hf}_{0.995}\text{Al}_{0.005}\text{O}_3$  were synthesized by the solid state method, pressed into pellets and sintered at 1800 °C for 20 h in vacuum; it was found that the addition of Al re-

sulted in the increase in density up to 98.9%. The use of spark plasma sintering (SPS) method was reported to be effective for fabrication of the high-density ceramics of strontium hafnate [30, 31]. The powder synthesized by the solid state method was poured into a graphite die, placed in a SPS chamber, stepwise heated to a high temperature (1600–1900 °C), and kept at this temperature for 45 min; the relative density of the obtained samples was more than 99%. It is obvious that the use of sintering technologies, based on long-term high-temperature annealing, sometimes under vacuum conditions, or on the SPS method, leads to a significant increase in the cost of ceramics. Consequently, the search for additives that promote better sintering of alkaline earth hafnates is relevant.

A positive effect of the partial substitution of hafnium by indium and tin on the sintering of  $\text{BaHf}_{0.9-x}\text{In}_x\text{Sn}_{0.1}\text{O}_{3-\delta}$  ( $x = 0.05\text{--}0.25$ ) ceramics was reported in [22]. It was shown that the introduction of indium alone made it possible to achieve a relative density of ~94%, while the co-doping led to an increase in density up to 96.25%. Isovalent substitution should also affect the ionic conductivity of oxides, in addition to their sinterability, due to the difference in ionic radii and the electronegativity of the host and dopant cations. It was shown in [35] that the introduction of tin into  $\text{BaZr}_{0.8}\text{Sc}_{0.2}\text{O}_{3-\delta}$  led to an increase in conductivity, although it was accompanied by a decrease in the average grain size in  $\text{BaZr}_{0.8-x}\text{Sn}_x\text{Sc}_{0.2}\text{O}_{3-\delta}$  ceramics from 0.97  $\mu\text{m}$  for  $x=0$  to 0.39  $\mu\text{m}$  for  $x=0.2$ . However, it is difficult to assess the effect of partial substitution of hafnium by tin on the sintering ability of  $\text{BaZr}_{0.8}\text{Sc}_{0.2}\text{O}_{3-\delta}$ , since the authors additionally introduced a sintering aid, 0.5 wt.% CuO, and did not analyze the change in density depending on the tin content.

To the best of the authors, knowledge, there are no data on the effect of Sn-doping on the sintering behavior and electrical properties of strontium hafnate. This research aims to study the effect of isovalent substitution of hafnium by tin in strontium hafnate on sinterability and electrical conductivity. The ceramic samples  $\text{SrHf}_x\text{Sn}_{1-x}\text{O}_{3-\delta}$  ( $x = 0\text{--}0.16$ ) were obtained by solid state synthesis, their phase composition and microstructure were studied by X-ray diffraction (XRD) and scanning electron microscopy (SEM), electrical conductivity was measured by the impedance method and the four-probe direct current (DC) method.

## 2. Experimental part

$\text{SrHf}_x\text{Sn}_{1-x}\text{O}_{3-\delta}$  ( $x = 0.04\text{--}0.16$ ) compositions were synthesized by the solid state reaction method using  $\text{HfO}_2$ ,  $\text{SrCO}_3$  and  $\text{SnO}_2$  (all with 99.9% purity) as precursors. The starting materials were preliminary dried at a temperature of 150 °C for 5 hours to remove adsorbed water, and then thoroughly mixed in a planetary mill (Retsch PM 100) in a calculated ratio. The synthesis was carried out at 1200 °C for 6 hours with intermediate regrinding. Then the powder was pressed into pellets under a pressure of 300 MPa

and sintered at a temperature of 1600 °C for 5 hours in air. A schematic diagram of the fabrication of  $\text{SrHf}_x\text{Sn}_{1-x}\text{O}_{3-\delta}$  samples is presented in Figure 1.

The apparent density of the samples was determined as the mass to volume ratio, which were determined by weighing and measuring the dimensions of the sample. The relative density was calculated as the ratio of measured to theoretical density. The phase composition and crystal structure of the sintered samples were studied using an X-ray diffractometer D-Max 2200 (Rigaku, Tokyo, Japan) in  $\text{Cu K}\alpha$  radiation within  $2\theta$  range from 20 to 80° at a scanning speed of 0.02 rpm with a step of 0.1°. The X-ray diffraction (XRD) measurements were performed at room temperature.

To study the microstructure of the samples by SEM, the surface of the samples was polished using diamond pastes and thermally etched at a temperature of 1200 °C for 4 hours in order to make the granular structure of ceramics visible. The microstructure of the samples was studied using a MIRA 3 LMU electron microscope (Tescan, Brno, Czech Republic).

Impedance measurements were performed on a Bio-Logic SP-200 impedance meter in the frequency range from 0.1 Hz to 1 MHz with an amplitude of 30 mV in dry air ( $p\text{H}_2\text{O} = 40$  Pa). For these measurements, platinum paste was symmetrically applied to the opposite faces of the  $\text{SrHf}_x\text{Sn}_{1-x}\text{O}_{3-\delta}$  pellets and sintered at 1000 °C (1 hour); the area of the Pt electrodes was 0.6  $\text{cm}^2$ . Dry air was obtained by blowing atmospheric air through a column filled with zeolite beads. The measurements were carried out in the temperature range of 550–800 °C. For the spectra analysis, the methods of equivalent circuits (ZView software) and distribution of relaxation times (DRT) (DRT-tools software) were applied.

To measure the electrical conductivity by the four-probe DC method, a sample in the form of a bar was cut out from the pellet. Four Pt wires were wound on to the sample to serve as current electrodes and potential probes. The distance between the potential probes was 0.75 cm, and the cross-sectional area of the sample was 0.05  $\text{cm}^2$ .

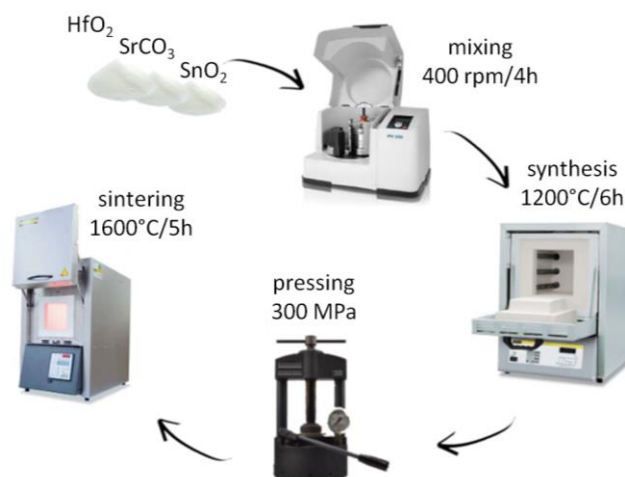


**Figure 1** Schematic diagram of  $\text{SrHf}_x\text{Sn}_{1-x}\text{O}_{3-\delta}$  ceramics fabrication.

Electrical conductivity  $\sigma$  was calculated using the following formula:

$$\sigma = \frac{US}{IL}, \quad (1)$$

where  $S$  and  $L$  are the cross-sectional area of the sample and the distance between the potential probes,  $I$  is the current, and  $U$  is the voltage.

The DC measurements were performed at 900 °C in the  $pO_2$ -range of  $10^{-18}$ –0.21 atm using a ZIRCONIA-318 regulator which ensured the automatical change and control of the oxygen partial pressure. The schematic view of the DC measurement setup is shown in Figure 2.

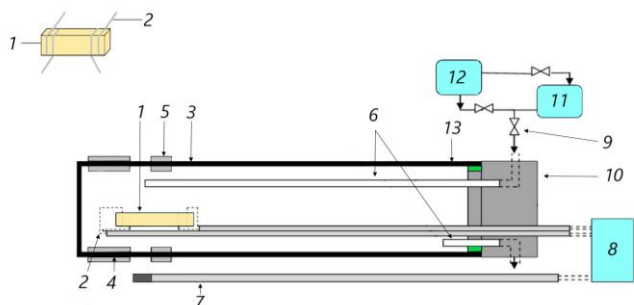


**Figure 2** Schematic view of DC measurement setup: 1 – sample, 2 – platinum wires, 3 – YSZ tube, 4 – electrochemical pump, 5 – electrochemical sensor, 6 – gas inlet and outlet tubes, 7 – thermocouple, 8 – Zirconia-318 regulator, 9 – valve, 10 – fluoroplastic plug, 11 – bubbler, 12 – gas cylinder or compressor, 13 – sealant.

### 3. Results and Discussion

#### 3.1. Characterization of the structure and morphology of the $SrHf_xSn_{1-x}O_{3-\delta}$ samples

Analysis of the XRD patterns of  $SrHf_xSn_{1-x}O_{3-\delta}$  sintered samples, which are presented in Figure 3a, showed that all the samples are single-phase and have the orthorhombic structure of  $SrHfO_3$  with the  $Pnma$  space group (ICDD 89-5605). No impurity phases were found in the samples. Figure 3b shows that Sn doping results in the peak shifting towards higher  $2\theta$  angles. A linear decrease in the unit cell volume with an increase in the tin content in strontium hafnate (Figure 3c) is consistent with the assumption that tin incorporates into the  $SrHfO_3$  crystal lattice, replacing hafnium, since the ionic radius of tin is 0.069 nm, and the ionic radius of hafnium is 0.071 nm. A schematic structure of  $SrHf_xSn_{1-x}O_{3-\delta}$  is presented in Figure 3d.

The morphology of  $SrHf_xSn_{1-x}O_{3-\delta}$  ceramic samples was evaluated from the SEM images displayed in Figure 4. As can be seen, the undoped strontium hafnate has a nanograin structure with an average grain size of ~100 nm, while Sn doping results in the grain growth: in the doped samples, the grain size varies from 1 to 5  $\mu m$ , and the morphology of the ceramics practically does not change with the tin content.

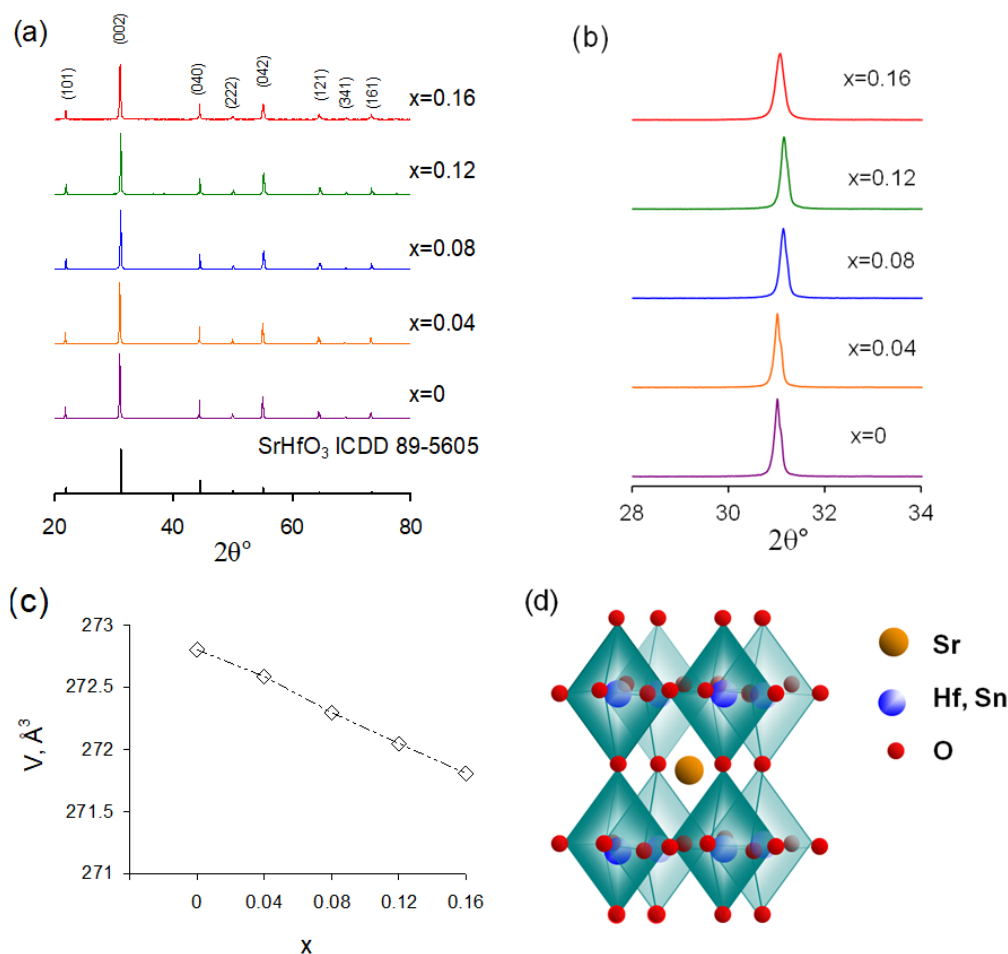


**Figure 3** XRD patterns of  $SrHf_xSn_{1-x}O_{3-\delta}$  (a), the magnified fragment of diffractograms showing (002) peak (b), unit cell volume of  $SrHf_xSn_{1-x}O_{3-\delta}$  as a function of Sn content (c), and schematic structure of  $SrHf_xSn_{1-x}O_{3-\delta}$  (d).

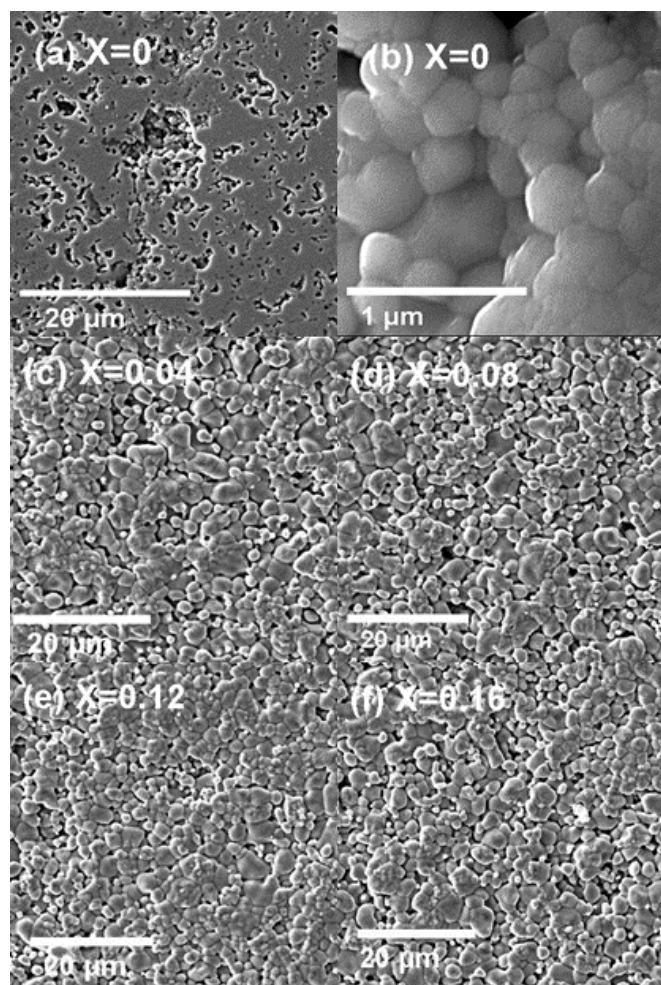


**Figure 4** SEM images of the surface of  $\text{SrHf}_x\text{Sn}_{1-x}\text{O}_{3-\delta}$  samples:  $x = 0$  (a, b),  $x = 0.04$  (c),  $x = 0.08$  (d),  $x = 0.12$  (e),  $x = 0.16$  (f).

The relative densities of the sintered  $\text{SrHf}_x\text{Sn}_{1-x}\text{O}_{3-\delta}$  samples are presented in Table 1. As can be seen, the introduction of 4 at.% Sn improves the sintering of ceramics, however, an increase in the tin concentration has practically no effect on their density, which is close to 80% for all Sn-doped samples. The relatively low density of the ceramics indicates that further efforts are needed to sinter the high-density strontium hafnate-based ceramics.

### 3.2. Electrical conductivity of $\text{SrHf}_x\text{Sn}_{1-x}\text{O}_{3-\delta}$

The impedance measurements of  $\text{SrHf}_x\text{Sn}_{1-x}\text{O}_{3-\delta}$  ( $x = 0.04-0.16$ ) samples were performed in the temperature range of 550–800 °C in dry ( $\text{pH}_2\text{O} = 40$  Pa) air. The impedance of the undoped  $\text{SrHfO}_3$  could not be measured because of its very high resistance. For illustration, the hodographs of  $\text{SrHf}_x\text{Sn}_{1-x}\text{O}_{3-\delta}$  measured in dry air at temperatures of 700–800 °C are shown in Figure 5a–d. Figure 5e presents the fitting of the spectrum on the basis of the equivalent circuit consisting of three RQ elements connected in series (R denotes a resistance, Q is a constant phase element), and the results of DRT analysis for the sample with  $x = 0.08$  at 700 °C. Taking into account the obtained characteristic capacitances, the high-frequency semicircle ( $C \sim 10^{-11}$  F  $\text{cm}^{-2}$ ) can be assigned to the response of grain interior of a sample, the medium-frequency semicircle

( $C \sim 10^{-8}$  F  $\text{cm}^{-2}$ ) is related to grain boundaries, and the low-frequency arc with a high capacitance ( $C \sim 10^{-3}$  F  $\text{cm}^{-2}$ ) is caused by the electrode processes.

As can be seen in Figure 5a–d, in the most of hodographs the grain boundary response is small compared to that of the bulk, which makes it difficult to reliably separate the grain boundary resistance; therefore, only the total resistance of the  $\text{SrHf}_x\text{Sn}_{1-x}\text{O}_{3-\delta}$  electrolytes was discussed. The conductivity of the samples was calculated as follows:

$$\sigma = \frac{h}{R_{el}S^2}, \quad (2)$$

where  $h$  is the thickness of a sample,  $S$  is the area of electrodes,  $R_{el}$  is the electrolyte resistance.

The Arrhenius dependences of conductivity presented in Figure 6 are nearly linear; the activation energy for all compositions is  $1.5 \pm 0.1$  eV. For comparison, the figure shows the conductivities of undoped strontium hafnate and strontium zirconate reported in [26, 36]. It can be seen that the substitution of hafnium by tin leads to an increase in conductivity by more than 2 orders of magnitude, e.g., the most conductive composition with  $x = 0.08$  exhibits a conductivity  $\sim 830$  times greater than undoped strontium hafnate at 600 °C, despite the fact that the density of the  $\text{SrHf}_x\text{Sn}_{1-x}\text{O}_{3-\delta}$  samples ( $\sim 80\%$ ) is significantly lower than the density of the  $\text{SrHfO}_3$  sample (95%), which was sintered at a much higher temperature of 1750 °C [36]. Figure 7 demonstrates the conductivity dependences of  $\text{SrHf}_x\text{Sn}_{1-x}\text{O}_{3-\delta}$  on the Sn concentration; as can be seen, the sample with  $x = 0.08$  has the highest conductivity, which is equal to  $4.1 \cdot 10^{-6}$  S  $\text{cm}^{-1}$  at 800 °C. However, the conductivity of  $\text{SrHf}_{0.92}\text{Sn}_{0.08}\text{O}_{3-\delta}$  sample is still lower than that of  $\text{SrZrO}_3$  by about an order of magnitude, as can be seen in Figure 6.

In general, an increase in ionic conductivity upon doping may be due to an increase in the concentration of charge carriers (oxygen vacancies in the case of oxide-ion conductors) and/or an increase in their mobility. The iso-valent substitution  $\text{Sn}^{4+} \rightarrow \text{Hf}^{4+}$  should not lead to the formation of additional oxygen vacancies; therefore, it can be assumed that the increase in conductivity upon Sn doping is related to the higher mobility of oxygen vacancies. However, the smaller radius of  $\text{Sn}^{4+}$  ion compared to the  $\text{Hf}^{4+}$  ion is expected to lower the mobility because of the narrowing of channels for oxide-ions migration, although the size factor should not lead to a noticeable effect at low dopant concentrations. Probably, it is the chemical nature of tin, namely, its electron configuration, which influences interatomic bonding and, accordingly, the mobility of charge carriers in  $\text{SrHf}_x\text{Sn}_{1-x}\text{O}_{3-\delta}$ .

**Table 1** Relative density of  $\text{SrHf}_{1-x}\text{Sn}_x\text{O}_{3-\delta}$  ceramic samples.

$x$	0	0.04	0.08	0.12	0.16
Relative density, %	75±2	82±2	79±2	79±2	82±2

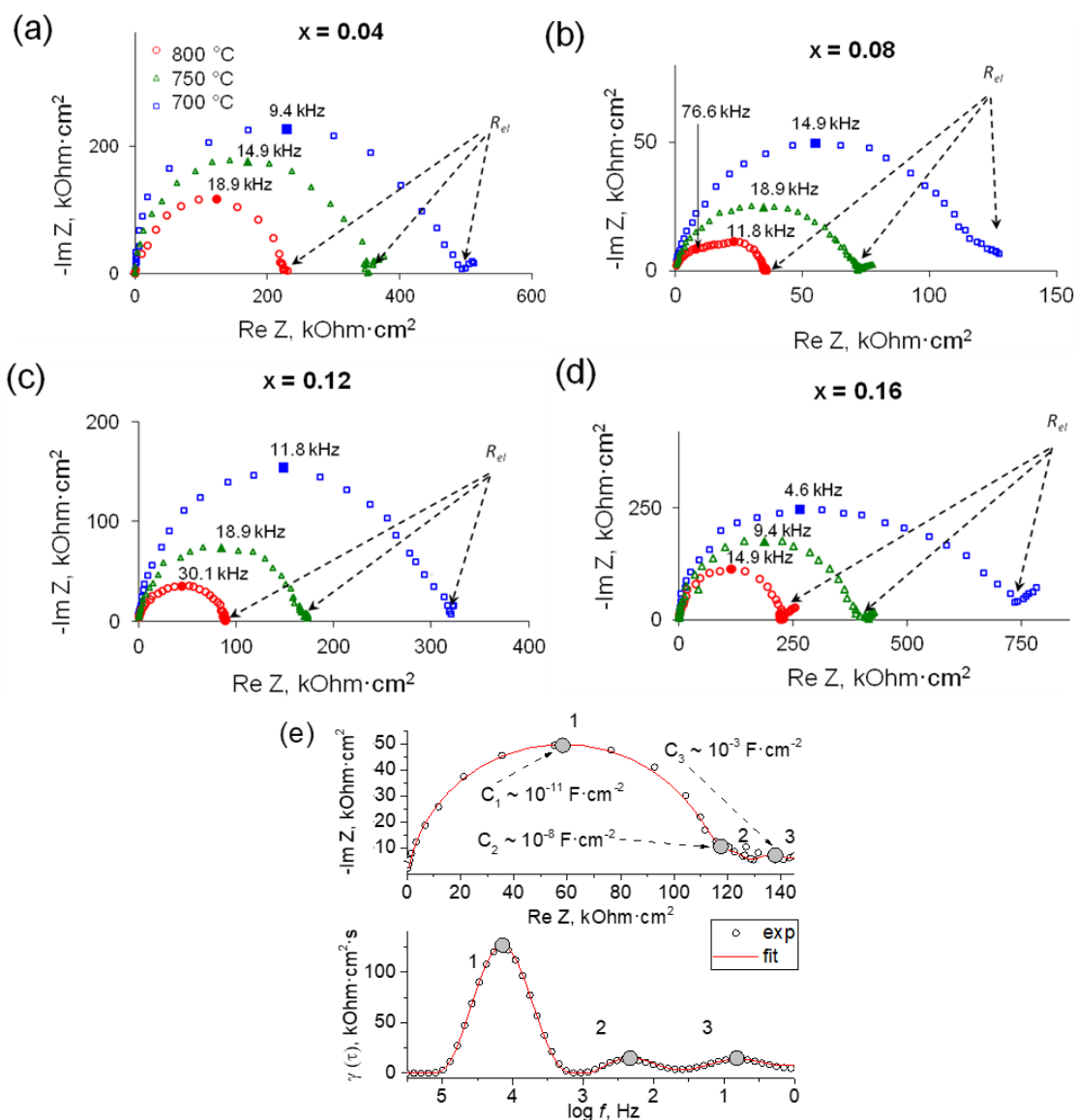


**Figure 5** Impedance spectra of  $\text{SrHf}_x\text{Sn}_{1-x}\text{O}_{3-\delta}$  in dry air:  $x = 0.04$  (a),  $x = 0.08$  (b),  $x = 0.12$  (c),  $x = 0.16$  (d), impedance with fitting and DRT spectra for  $\text{SrHf}_{0.92}\text{Sn}_{0.08}\text{O}_{3-\delta}$  at  $700\text{ }^\circ\text{C}$  (e).

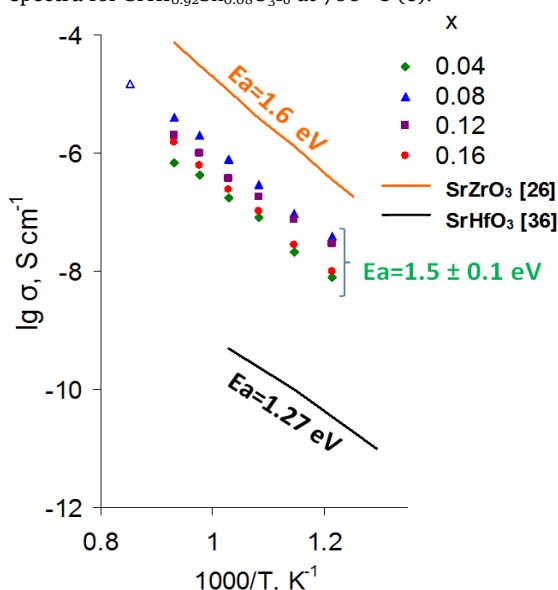


**Figure 6** Arrhenius plots of  $\text{SrHf}_x\text{Sn}_{1-x}\text{O}_{3-\delta}$  conductivity in dry air. Solid lines show the conductivity of  $\text{SrZrO}_3$  [26] and  $\text{SrHfO}_3$  [36]. The open triangle is the conductivity of the sample with  $x = 0.08$  measured by the four-probe DC method.

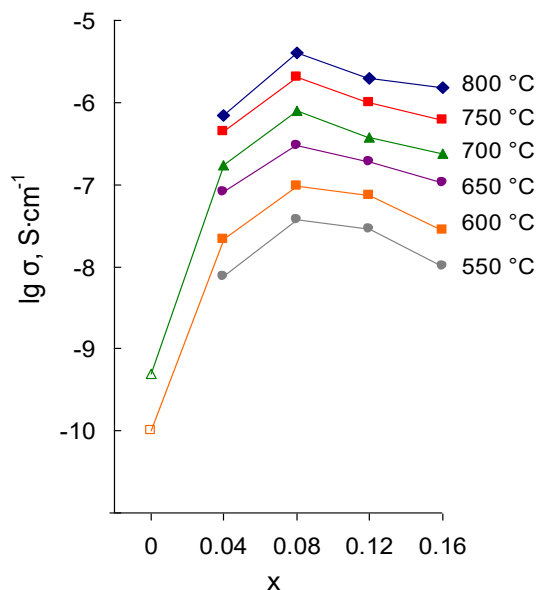
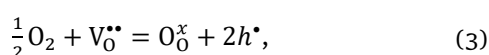


**Figure 7** Conductivity of  $\text{SrHf}_x\text{Sn}_{1-x}\text{O}_{3-\delta}$  as a function of Sn-content in dry air. Open symbols are the conductivity of  $\text{SrHfO}_3$  reported in [36].

In addition, it can be assumed that the very thin film of tin oxide is formed at the grain boundaries of doped strontium hafnate, which is undetectable by the conventional X-ray diffraction and microscopy methods. The impedance data are consistent with this assumption: the response of grain boundaries is not visible in the most of hodographs, which indicates that the contribution of boundaries to the total resistance of the samples is very small (Figure 5 a-d). Probably, the existence of the film of tin oxide results in a decrease of the resistance of grain boundaries, which is known to be one of the main reasons for the low conductivity of the related perovskites based on strontium zirconate [26, 37], and, as a result, the total conductivity of the Sn-doped samples increases. However, further studies are needed to establish the mechanism of the effect of Sn doping on the electrical conductivity of strontium hafnate.

To determine the type of charge carriers, the conductivity of SrHf<sub>0.92</sub>Sn<sub>0.08</sub>O<sub>3-δ</sub> sample, which exhibits the highest conductivity, as a function of pO<sub>2</sub> was studied using the four-probe DC method. Due to the high resistance of the sample, the measurements were carried out at a high temperature of 900 °C. As can be seen in Figure 8, the conductivity increases with increasing pO<sub>2</sub> under oxidizing conditions (pO<sub>2</sub> > 10<sup>-5</sup> atm), while a wide plateau is observed in reducing atmospheres (10<sup>-18</sup>–10<sup>-5</sup> atm). The value of conductivity at the plateau is considered an oxide-ion conductivity, which is independent of pO<sub>2</sub>. An increase in conductivity at high pO<sub>2</sub> is typically related to generation of oxygen holes upon oxygen incorporation into oxide lattice according to the generally accepted mechanism of defect formation. In this mechanism, the equilibrium between gaseous oxygen, oxygen ions, oxygen vacancies and holes in oxide-ion conducting oxides in oxidizing atmospheres can be represented in terms of Kröger-Vink notation as follows:



The electroneutrality condition for reaction 3 can be written as follows:

$$h^{\bullet} = 2[V_O^{\bullet\bullet}]. \quad (4)$$

Taking into account the electroneutrality condition (Equation 4) and the mass action law for Equation 3 one can derive that the hole concentration is proportional to  $pO_2^{1/6}$ . As long as the hole conductivity is proportional to the hole concentration, the slope of the log σ – log pO<sub>2</sub> dependence is to be equal to 1/6. However, the slope of the experimentally obtained dependence shown in Figure 8 is lower, which can be caused by different reasons. First, in the transition region, in which the oxide-ion and hole conductivities are comparable, the slope may vary from zero to 1/6. Second, the tin oxide film, which is supposedly formed on the surface of grains in SrHf<sub>x</sub>Sn<sub>1-x</sub>O<sub>3-δ</sub> may hinder the oxygen incorporation (Reaction 3) and the hole generation.

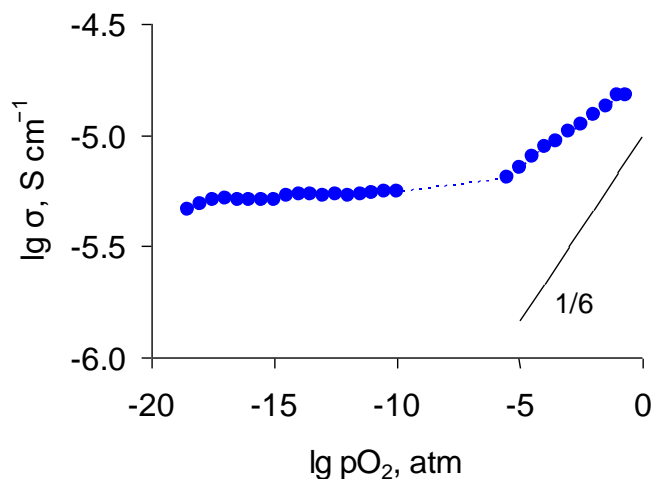


**Figure 8** Conductivity of SrHf<sub>0.92</sub>Sn<sub>0.08</sub>O<sub>3-δ</sub> as a function of pO<sub>2</sub> at 900 °C.

Thus, based on the conductivity dependence on pO<sub>2</sub>, it can be concluded that in Sn-doped strontium hafnate oxide-ion conductivity dominates in a wide range of pO<sub>2</sub>, while the hole conductivity appears under oxidizing conditions. The transference number of ions  $t_i$  can be evaluated from the log σ – log pO<sub>2</sub> dependence as a ratio of the ionic conductivity, which is the conductivity on the plateau, to the conductivity at any value of pO<sub>2</sub>; e.g., for SrHf<sub>0.92</sub>Sn<sub>0.08</sub>O<sub>3-δ</sub> at 900 °C,  $t_i = 0.35$  in air and gradually increases with decreasing pO<sub>2</sub>, approaching unity at pO<sub>2</sub> of 10<sup>-6</sup> atm.

#### 4. Limitations

Sn doping improves the density of SrHfO<sub>3</sub>-based ceramic samples; however, the resulting ceramic is not sufficiently dense for application in electrochemical cells, such as fuel cells or electrolysis cells, which require the use of a gas-tight electrolyte. Our further research aims at the fabrication of high-density ceramics by using nanopowders and sintering aids, and manufacturing and testing fuel and electrolysis cells.

#### 5. Conclusions

In the present research, the effect of isovalent substitution of hafnium by tin in strontium hafnate on sinterability and electrical conductivity was considered. SrHf<sub>x</sub>Sn<sub>1-x</sub>O<sub>3-δ</sub> (x = 0–0.16) ceramic samples were obtained by the solid-phase method. All samples were found to be phase pure and have the orthorhombic structure of SrHfO<sub>3</sub> with *Pnma* space group. The Sn doped samples sintered at a temperature of 1600 °C for 5 hours exhibited a higher relative density (80±2%) compared to the undoped sample (75±2%). The grain size increased from ~100 nm to 1–5 μm upon the Sn-doping. The study of conductivity revealed that the substitution of hafnium by tin leads to an increase in conductivity, and the highest conductivity (4.1·10<sup>-6</sup> S cm<sup>-1</sup> at 800 °C in dry air) is observed for the sample with x = 0.08. The conductivity of

SrHf<sub>0.92</sub>Sn<sub>0.08</sub>O<sub>3-δ</sub> is ~830 times greater than that of the undoped strontium hafnate at 600 °C. The activation energy of the conductivity of SrHf<sub>x</sub>Sn<sub>1-x</sub>O<sub>3-δ</sub> is 1.5±0.1 eV. The dependence of conductivity on the oxygen partial pressure indicates that the oxide-ion conductivity dominates in a wide range of pO<sub>2</sub>, while the hole conductivity appears under oxidizing conditions. For SrHf<sub>0.92</sub>Sn<sub>0.08</sub>O<sub>3-δ</sub> composition, the transference number of ions in air was 0.35 at 900 °C. It is not clear why the isovalent substitution gives a significant increase in conductivity; further research using the high-resolution electron microscopy and energy-dispersive X-ray spectroscopy methods is needed for understanding the mechanism of the Sn-doping effect on the properties of strontium hafnate.

### • Supplementary materials

No supplementary materials are available.

### • Funding

This research had no external funding.

### • Acknowledgments

SEM and XRD experiments were done using the facilities of the shared access centre "Composition of compounds" (Institute of High-Temperature Electrochemistry, Ural Branch of the Russian Academy of Sciences). The authors are grateful to Artem Tarutin for the help with the measurements of conductivity by the DC 4-probe method.

### • Author contributions

Conceptualization: L.A.D.

Visualization: A.S.K.

Investigation: A.S.K., A.N.M.

Methodology: L.A.D., A.S.K, A.N.M.

Supervision: L.A.D.

Writing – original draft: A.S.K.

Writing – review & editing: L.A.D.

### • Conflict of interest

The authors declare no conflict of interest.

### • Additional information

Author IDs:

Adelya S. Khaliullina, Scopus ID [57206712878](https://orcid.org/0000-0002-5720-6712);

Anastasia N. Meshcherskikh, Scopus ID [56784365300](https://orcid.org/0000-0002-5678-4365);

Liliya A. Dunyushkina, Scopus ID [6507914539](https://orcid.org/0000-0002-6507-9145).

Website:

Institute of High Temperature Electrochemistry UB  
RAS, <http://www.ihte.uran.ru>.

## References

- Hwang SC, Choi GM. The mixed ionic and electronic conductivity of CaZrO<sub>3</sub> with cation nonstoichiometry and oxygen partial pressure. *Solid State Ionics*. 2008;179:1042–1045. doi:[10.1016/j.ssi.2007.11.034](https://doi.org/10.1016/j.ssi.2007.11.034)
- Wang C, Xu X, Yu H, Wen Y, Zhao K. A study of the solid electrolyte Y<sub>2</sub>O<sub>3</sub> doped CaZrO<sub>3</sub>. *Solid State Ionics*. 1988;28–30:542–545. doi:[10.1016/so167-2738\(88\)80099-7](https://doi.org/10.1016/so167-2738(88)80099-7)
- Yugami H, Naito H, Arashi H. Fabrication of SrMoO<sub>3</sub>, (M = Ce and Zr) thin films and SrCeO<sub>3</sub>/SrZrO<sub>3</sub>, superlattices by laser ablation. *Appl Surf Sci*. 1997;113–114:222–226. doi:[10.1016/S0169-4332\(96\)00899-9](https://doi.org/10.1016/S0169-4332(96)00899-9)
- Saini DS, Bhattacharya D. Electrical properties of BaZrO<sub>3</sub> Ceramic synthesized by a flash pyrolysis process. *AIP Conf Proceed*. 2016;1724:020104-1–020104-8. doi:[10.1063/1.4945224](https://doi.org/10.1063/1.4945224)
- Nomura K, Kageyama H. Transport properties of Ba(Zr<sub>0.8</sub>Y<sub>0.2</sub>)O<sub>3-δ</sub> perovskite. *Solid State Ionics*. 2007;178:661–665. doi:[10.1016/j.ssi.2007.02.010](https://doi.org/10.1016/j.ssi.2007.02.010)
- Weng Z, Huang H, Li X, Zhang Y, Shao R, Yi Y, Lu Y, Zeng X, Zou J, Chen L, Li W, Meng Y, Asefa T, Huang C. Coordination Tailoring of epitaxial perovskite-derived iron oxide films for efficient water oxidation electrocatalysis. *ACS Catalysis*. 2023;13(4):2751–2760. doi:[10.1021/acscatal.2c05147](https://doi.org/10.1021/acscatal.2c05147)
- Farooq N, Luque R, Len T, Osman SM, Qureshi AM, Nazir MA, ur Rehman A. Design of SrZr<sub>0.1</sub>Mn<sub>0.4</sub>Mo<sub>0.4</sub>Y<sub>0.1</sub>O<sub>3-δ</sub> heterostructured with ZnO as electrolyte material: structural, optical and electrochemical behavior at low temperatures. *Ceram Int*. 2023;49(2):2174–2182. doi:[10.1016/j.ceramint.2022.09.184](https://doi.org/10.1016/j.ceramint.2022.09.184)
- Iwahara H, Esaka T, Uchida H, Maeda N. Proton conduction in sintered oxides and its application to steam electrolysis for hydrogen production. *Solid State Ionics*. 1981;3–4:359–363. doi:[10.1016/0167-2738\(81\)90113-2](https://doi.org/10.1016/0167-2738(81)90113-2)
- Iwahara H, Uchida H, Tanaka S. High temperature type proton conductor based on SrCeO<sub>3</sub> and its application to solid electrolyte fuel cells. *Solid State Ionics*. 1983;9–10:1021–1025. doi:[10.1016/0167-2738\(83\)90125-X](https://doi.org/10.1016/0167-2738(83)90125-X)
- Iwahara H, Uchida H, Maeda N. High temperature fuel and steam electrolysis cells using proton conductive solid electrolytes. *J Power Sources*. 1982;7(3):293–301. doi:[10.1016/0378-7753\(82\)80018-9](https://doi.org/10.1016/0378-7753(82)80018-9)
- Takahashi T, Iwahara H. Solid state ionics: proton conduction in perovskite type solid solutions. *Rev Chim Miner*. 1980;17(4):243–253. doi:[10.1002/chin.198114014](https://doi.org/10.1002/chin.198114014)
- Sammes N, Phillips R, Smirnova A. Proton conductivity in stoichiometric and sub-stoichiometric yttrium doped SrCeO<sub>3</sub> ceramic electrolytes. *J Power Sources*. 2004;134(2):153–159. doi:[10.1016/j.jpowsour.2004.02.036](https://doi.org/10.1016/j.jpowsour.2004.02.036)
- LÜ J, Wang L, Fan L, Li Y, Dai L, Guo H. Chemical stability of doped BaCeO<sub>3</sub>–BaZrO<sub>3</sub> solid solutions in different atmospheres. *J Rare Earths*. 2008;26:505–510. doi:[10.1016/S1002-0721\(08\)60127-1](https://doi.org/10.1016/S1002-0721(08)60127-1)
- Choi SM, Lee JH, Choi MB, Hong J, Yoon KJ, Kim BK, Lee HW, Lee JH. Determination of electronic and ionic partial conductivities of BaCeO<sub>3</sub> with Yb and In doping. *J Electrochem Soc*. 2015;162(7):F789–F795. doi:[10.1149/2.0011508jes](https://doi.org/10.1149/2.0011508jes)
- Shrivastava UN, Duncan KL, Chung JN. Experimentally validated numerical modeling of Eu doped SrCeO<sub>3</sub> membrane for hydrogen separation. *Int J Hydrog Energy*. 2012;37(20):15350–15358. doi:[10.1016/j.ijhydene.2012.07.061](https://doi.org/10.1016/j.ijhydene.2012.07.061)
- Zhang C, Zhao H, Zhai S. Electrical conduction behavior of proton conductor BaCe<sub>1-x</sub>Sm<sub>x</sub>O<sub>3-δ</sub> in the intermediate temperature range. *Int J Hydrogen Energy*. 2011;36(5):3649–3657. doi:[10.1016/j.ijhydene.2010.12.087](https://doi.org/10.1016/j.ijhydene.2010.12.087)
- Janke D. Oxygen probes based on calcia-doped hafnia or calcium zirconate for use in metallic melts. *Metall Trans B*. 1982;13B:227–235. doi:[10.1007/BF02664579](https://doi.org/10.1007/BF02664579)
- Bhide SV, Virkar AV. Stability of AB<sup>1</sup>/2B<sup>1</sup>/2O<sub>3</sub>-type mixed Perovskite proton conductors. *J Electrochem Soc*. 1999;146(12):4386–4392. doi:[10.1149/1.1392648](https://doi.org/10.1149/1.1392648)

19. Kato K, Han D, Uda T. Transport properties of proton conductive Y-doped BaHfO<sub>3</sub> and Ca or Sr-substituted Y-doped BaZrO<sub>3</sub>. *J Am Ceram Soc.* 2019;102(3):1201–1210. doi:[10.1111/jace.15946](https://doi.org/10.1111/jace.15946)
20. Sun W, Zhu Z, Shi Z, Liu W. Chemically stable and easily sintered high-temperature proton conductor BaZr<sub>0.8</sub>In<sub>0.2</sub>O<sub>3-δ</sub> for solid oxide fuel cells. *J Power Sources.* 2013;229:95–101. doi:[10.1016/j.jpowsour.2012.12.017](https://doi.org/10.1016/j.jpowsour.2012.12.017)
21. Snijkers FMM, Buekenhoudt A, Luyten JJ, Coymans J, Mertens M. Proton conductivity in perovskite type yttrium doped barium hafnate. *Scr Mater.* 2004;51:1129–1134. doi:[10.1016/j.scriptamat.2004.08.021](https://doi.org/10.1016/j.scriptamat.2004.08.021)
22. Yang W, Wang L, Li Y, Zhou H, He Z, Han C, Dai L. An easily sintered, chemically stable indium and tin co-doped barium hafnate electrolyte for hydrogen separation. *J Alloys Compd.* 2021;868:159117. doi:[10.1016/j.jallcom.2021.159117](https://doi.org/10.1016/j.jallcom.2021.159117)
23. Bevilion E, Hermet J, Dezanneau G, Geneste G. How dopant size influences the protonic energy landscape in BaSn<sub>1-x</sub>M<sub>x</sub>O<sub>3-x/2</sub> (M = Ga, Sc, In, Y, Gd, La). *J. Mater Chem A.* 2014;2(2):460–471. doi:[10.1039/c3ta12870a](https://doi.org/10.1039/c3ta12870a)
24. Loken A, Kjolseth C, Haugsrud R. Electrical conductivity and TG-DSC study of hydration of Sc-doped CaSnO<sub>3</sub> and CaZrO<sub>3</sub>. *Solid State Ionics.* 2014;267:61–67. doi:[10.1016/j.ssi.2014.09.006](https://doi.org/10.1016/j.ssi.2014.09.006)
25. Gorelov VP, Balakireva VB, Kuz'min AV. Ion conductivity of perovskites CaZr<sub>1-x</sub>Sc<sub>x</sub>O<sub>3-a</sub> (x=0.03–0.20) in hydrogen-containing atmospheres. *Russ J Electrochem.* 2016;52:1076–1081. doi:[10.1134/S1023193516110069](https://doi.org/10.1134/S1023193516110069)
26. Dunyushkina L, Khaliullina A, Meshcherskikh A, Pankratov A, Osinkin D. Effect of A-Site nonstoichiometry on defect chemistry and electrical conductivity of undoped and Y-doped SrZrO<sub>3</sub>. *Mater.* 2019;12:1258. doi:[10.3390/ma12081258](https://doi.org/10.3390/ma12081258)
27. Qian K, Pan Y, Hu Z, Chen X, Shi Y, Liu X, Chen H, Nikl M, Li J. Influence of co-doped alumina on the microstructure and radioluminescence of SrHfO<sub>3</sub>:Ce ceramics. *J Eur Ceram Soc.* 2020;40:449–455. doi:[10.1016/j.jeurceramsoc.2019.09.034](https://doi.org/10.1016/j.jeurceramsoc.2019.09.034)
28. Jarý V, Bohacek P, Pejchal J, Beitlerova A, Trunda B, Panek D, Bruza P, Kurosawa S, Yoshikawa A, Nikl M. Scintillating ceramics based on non-stoichiometric strontium hafnate. *Opt Mater.* 2018;77:246–252. doi:[10.1016/j.optmat.2018.01.042](https://doi.org/10.1016/j.optmat.2018.01.042)
29. Kurosawa S, Pejchal J, Wakahara S, Yokota Y, Yoshikawa A. Optical properties and radiation response of Ce:SrHfO<sub>3</sub> prepared by the spark plasma sintering method. *Rad Measur.* 2013;56:155–158. doi:[10.1016/j.radmeas.2013.01.051](https://doi.org/10.1016/j.radmeas.2013.01.051)
30. Khaliullina A, Meshcherskikh A, Pankratov A, Dunyushkina L. Effect of Sr deficiency on electrical conductivity of Yb-doped strontium zirconate. *Mater.* 2022;15: 4126. doi:[10.3390/ma15124126](https://doi.org/10.3390/ma15124126)
31. Yamanaka S, Maekawa T, Muta H, Matsuda T, Kobayashi S, Kurosaki K. Thermophysical properties of SrHfO<sub>3</sub> and SrRuO<sub>3</sub>. *J Solid State Chem.* 2004;177(10):3484–3489. doi:[10.1016/j.jssc.2004.05.039](https://doi.org/10.1016/j.jssc.2004.05.039)
32. Thomas JK, Padma Kumar H, Prasad VS, Solomon S. Structure and properties of nanocrystalline BaHfO<sub>3</sub> synthesized by an auto-igniting single step combustion technique. *Ceram Int.* 2011;37(2):567–571. doi:[10.1016/j.ceramint.2010.10.005](https://doi.org/10.1016/j.ceramint.2010.10.005)
33. Yang W, Han C, Li Y, Zhou H, Liu S, Wang L, He Z, Dai L. Influence of rare-earth doping on the phase composition, sinterability, chemical stability and conductivity of BaHf<sub>0.8</sub>Ln<sub>0.2</sub>O<sub>3-d</sub> (Ln=Yb, Y, Dy, Gd) proton conductors. *Int J Hydrog Energy.* 2021;46:35678–35691. doi:[10.1016/j.ijhydene.2021.08.093](https://doi.org/10.1016/j.ijhydene.2021.08.093)
34. Ma W, Li P, Dong H, Bai Y, Zhao J, Fan X. Y<sub>2</sub>O<sub>3</sub> and Yb<sub>2</sub>O<sub>3</sub> co-doped strontium hafnate as a new thermal barrier coating material. *J Therm Spray Technol.* 2013;23(1):154–159. doi:[10.1007/s11666-013-0006-9](https://doi.org/10.1007/s11666-013-0006-9)
35. Zvonareva IA, Kasyanova AV, Tarutin AP, Vdovin GK, Lyagaeva JG, Medvedev DA. Enhanced transport properties of Sn-substituted proton-conducting BaZr<sub>0.8</sub>Sc<sub>0.2</sub>O<sub>3-δ</sub> ceramic materials. *J Am Ceram Soc.* 2021;105(3):2105–2115. doi:[10.1111/jace.18224](https://doi.org/10.1111/jace.18224)
36. Lukin ES, Soyuzova AY. The synthesis, sintering, and properties of strontium hafnate. *Refractories.* 1973;14:174–180. doi:[10.1007/BF01286429](https://doi.org/10.1007/BF01286429)
37. Dunyushkina LA, Khaliullina ASH, Meshcherskikh AN, Pankratov AA. Sintering and conductivity of Sc-doped CaZrO<sub>3</sub> with Fe<sub>2</sub>O<sub>3</sub> as a sintering aid. *Ceram Int.* 2021;47:10565–10573. doi:[10.1016/j.ceramint.2020.12.168](https://doi.org/10.1016/j.ceramint.2020.12.168)